ELSEVIER

Dyes and Pigments, Vol. 39, No. 4, pp. 231–241, 1998

Printed in Great Britain
PII: S0143-7208(98)00011-4 0143-7208/98 $—see front matter

Photoelectric Properties of Amphiphilic Porphyrin Langmuir–Blodgett Film

Xuezhong He, Yalin Zhou, Lingxuan Wang, Tiankai Li, Zhichu Bi, Manhua Zhang* & Tao Shen

Institute of Photographic Chemistry, The Chinese Academy of Science, Beijing 100101, People's Republic of China

(Received 8 January 1998; accepted 27 January 1998)

ABSTRACT

The photovoltaic behavior of an electrochemical cell of $TC_{16}PyP(4)$ monolayer, deposited on SnO_2 optically transparent electrodes (SnO_2 OTE) by the Langmuir–Blodgett (LB) technique was investigated. The photocell was able to generate photocurrent, which increase in the presence of electron donors or acceptors in the KCl electrolyte solution, indicating that the photovoltaic effect of $TC_{16}PyP(4)$ perhaps originates from the photo-induced charge transfer between $TC_{16}PyP(4)$ molecules and SnO_2 semi-conductor. Moreover, the orientation of $TC_{16}PyP(4)$ in monolayer or LB films was also studied by π–A isotherm and polarized absorption spectrum. The result showed that the porphyrin macroring was oriented with an angle of about 25° against the aqueous surface as well as the substrate plane. © *1998 Elsevier Science Ltd. All rights reserved*

Keywords: amphiphilic porphyrin, LB films, photovoltaic effect, SnO_2 OTE, photo-induced charge transfer.

1 INTRODUCTION

In recent years, a number of organic compounds have been studied as potential sensitizers for light energy conversion into electric [1,2] or chemical

*Corresponding author. Fax: 086 106 202 9375.

energy [3]. Solar cells made from organic materials have received increasing interest due mainly to their low cost and ease of fabrication. These organic semi-conductors were often used for electrophotography in the form of thin film [4]. The frequently used methods for thin film include vacuum evaporation, spin-coating, dispersion in a polymer binder, and Langmuir–Blodgett film (LB film) techniques. The latter allows functional molecules to be arranged in a highly ordered structure on a solid substrate, and offers the possibility of practical application in electric devices.

Porphyrin, being thermally and chemically stable, has been widely used in this respect. As far as film-forming materials are concerned, the use of porphyrin for such studies has two main advantages, viz.: (i) one can obtain molecules with various molecular structures, and (ii) porphyrins are generally less sensitive to photodegradation [5]. We have been studying the photophysical and photochemical properties of porphyrins LB films with the aim of constructing molecular electronic devices. In this paper, we have employed symmetrically substituted porphyrin $TC_{16}PyP(4)$ as a film-forming material and studied the photoelectric properties of the $TC_{16}PyP(4)$ LB film. We have also studied the orientation of the $TC_{16}PyP(4)$ macroring in LB films by polarized UV-visible spectroscopy.

2 EXPERIMENTAL

2.1 Materials

The synthesis of the porphyrin amphiphiles was accomplished by quaternization of appropriate TPyP with 1-bromohexadecane [6]. Okuno *et al.* [6]

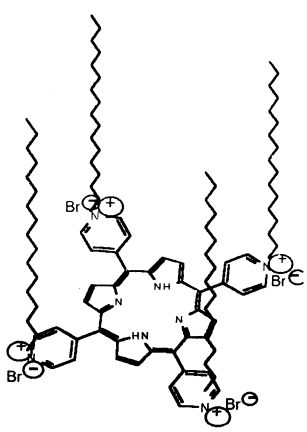

Fig. 1. Structure of $TC_{16}PyP(4)$.

obtained the pure product by repeated gel chromotagraphy over Sephadex LH-20. In this study, the purifications were made via fractionated crystallizations in CH_3OH, and then chromatography on a silica gel column using CH_2Cl_2/CH_3OH(9:1) as the eluent.

Elemental analysis: $TC_{16}PyP(4)$; Calc. (%), $C_{104}H_{158}Br_4N_8$, C, 67.90; H, 8.60; N, 6.09; Found (%), $C_{104}H_{158}Br_4N_8 \cdot 5H_2O$, C, 64.63; H, 8.71, N, 5.80.

All the other reagent were of analytical grade.

2.2 Monolayer and LB film method

Monolayer formation and deposition were carried on a Joyle–Loebel Langmuir Tough 4 under room temperature ($20 \pm 1^{\circ}C$). The surface pressure was measured by the Wilhelmy method. Triple-distilled deionized water (pH = 6) was used as subphase. The spreading solution of $TC_{16}PyP(4)$ in chloroform was spread onto the subphase using a microsyringe; when the solvent had evaporated thoroughly, compression began and the curve was recorded. The concentration of $TC_{16}PyP(4)$ was kept 1×10^{-4} mol L^{-1} in all the spreading solutions. The multilayers were deposited on quartz slides for electronic absorption spectra, and SnO_2 OTE for photovoltaic measurements, respectively. All the experiments for monolayer deposition were performed under surface pressures of 30 mN m^{-1}, unless otherwise stated. The dipping speed was 2 mm min^{-1}, resulting in a fairly good deposition of a typical Y-mode film with a transfer of 1.02.

2.3 Electronic absorption spectra

UV-vis absorption spectra were recorded on a Shimadzu UV-160A spectrophotometer; polarized UV-vis absorption spectra were recorded on a Hitachi 557 spectrophotometer with a polarizer.

2.4 Photoelectrochemical measurements

The experimental set-up used for the photoelectrochemical measurements is shown in Fig. 2. The electrochemical cell was made up of the bicell, which was linked by an agar salt bridge in order to increase the photovoltaic signal/noise ratio. A 500 W Xenon arc lamp was used as the light source. The blank photocurrent due to the SnO_2 OTE excitation had a measurable value at wavelengths below 390 nm; for illumination with wavelengths above 390 nm, a cut-off filter was used. The intensity of incident light was 80 mW cm^{-2}. The photocurrent and photovoltage were measured with a picoammeter and potentiostat, respectively. The photovoltaic signals were recorded by a computer for data treatment. The supporting electrolyte was 0.1 M KCl; where

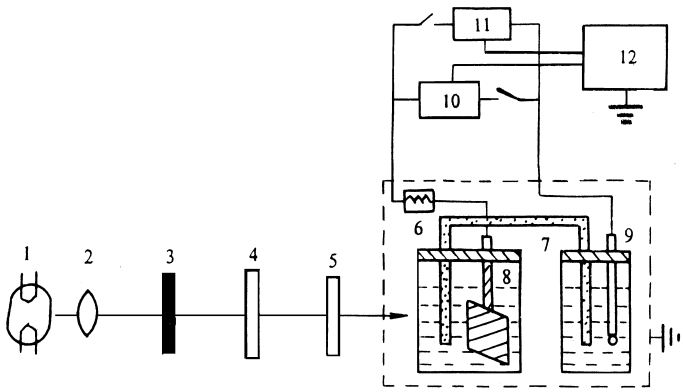

Fig. 2. Schematic diagram of the set-up for the photocurrent measurement. 1, Light source; 2, focusing lens; 3, shutter; 4, cut-off filter; 5, filter; 6, resistance; 7, agar salt bridge; 8, $TC_{16}PyP(4)$-deposited SnO_2 OTE; 9, SCE; 10, picoammeter; 11, potentiostat; 12, computer for data.

necessary, electron donors or acceptor could be contained. A saturated calomel electrode (SCE) was used as reference electrode. The electrochemical cell thus prepared, as well as all the electrical cables, were shielded with a common ground against electromagnetic perturbations. The experimental photovoltaic cell can be shown as: SnO_2 OTE/$TC_{16}PyP(4)$ LB films/0.1 M KCl aqueous solution/Agar salt bridge/saturated KCl solution, SCE.

3 RESULTS AND DISCUSSION

3.1 π–A isotherm measurement

Figure 3 shows the π–A isotherm of $TC_{16}PyP(4)$ on the pure water subphase at 20°C. There is distinct phase transition and an abrupt increase in slope, and no well-defined collapse was observed up to 50 mN m^{-1}, the limit of our apparatus, indicating that $TC_{16}PyP(4)$ can form stable monolayers at the air/water interface. At surface pressure around 30 mN m^{-1}, the monomolecular area (extrapolating the line part of π–A isotherm to the abscissa) is 2.20 nm^2. Based on the Corey–Pauling–Koltum (CPK) molecular model [7], one expects a molecular area of about 2.40 nm^2 if the porphyrin ring is oriented parallel to the aqueous surface, and of about 1.10 nm^2 if it is oriented perpendicular to the aqueous surface. Compared with the value of 2.20 nm^2 obtained from the π–A isotherm, we inferred that the porphyrin ring is oriented with an angle of 24° against the aqueous surface as well as the substrate plane.

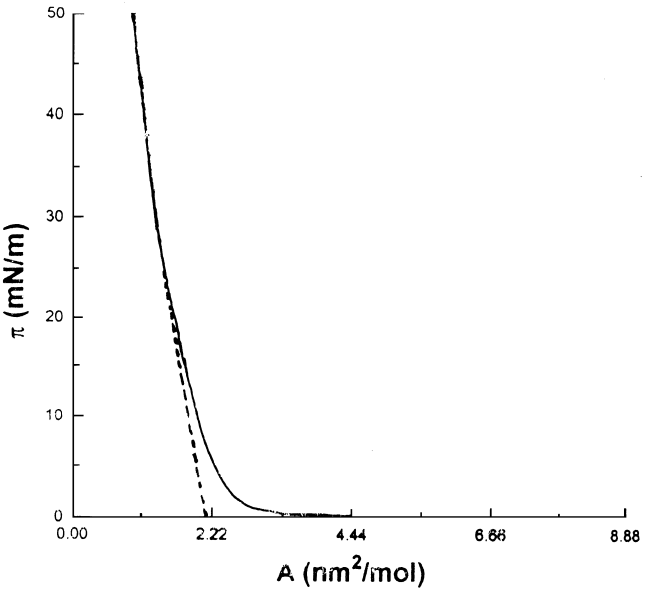

Fig. 3. π-A isotherm of $TC_{16}PyP(4)$ monolayer.

3.2 Orientation of $TC_{16}PyP(4)$ molecules

Figure 4 compares the absorption spectrum of the $TC_{16}PyP(4)$ LB film (solid line) with that of $TC_{16}PyP(4)$ chloroform solution (dashed line). In the case of the $TC_{16}PyP(4)$ LB film (38 layers), there are five absorption bands corresponding to those in solution, respectively. But, these absorption bands are broadened and red shifted, indicating the occurrence of interlayer interaction between porphyrin molecules. Moreover, as shown in the insert of Fig. 4, measurement of the Soret band absorbance of the $TC_{16}PyP(4)$ LB films at 435 nm vs the number of layers results in a straight line, indicating that the monolayer at the air/water interface could be well transferred onto the substrate during sequential dipping process.

In order to evaluate the orientation of $TC_{16}PyP(4)$ molecules in the LB films, polarized absorption spectra of the $TC_{16}PyP(4)$ LB films were measured. Typical polarized spectra illustrated in Fig. 4(a) for $\beta' = 0°$ and Fig. 4(b) for $\beta' = 45°$. In each figure, the solid and dashed lines indicate the absorption spectra for polarization vectors perpendicular and parallel to the dipping direction, respectively. If the plane of the porphyrin macroring were tilted from the substrate, there would be an inequality in the absorbance for the two polarization beams. As shown in Fig. 5, there are significant differences between the absorbance of perpendicular and parallel polarization,

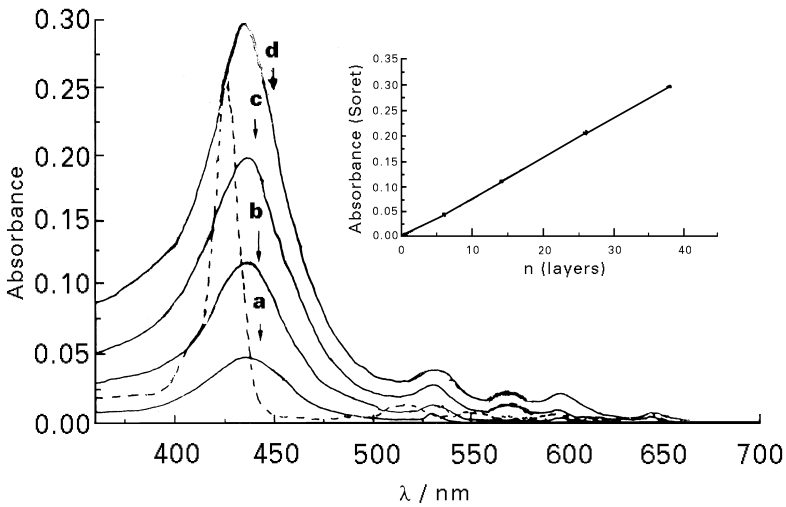

Fig. 4. UV-vis spectra of $TC_{16}PyP(4)$ in $CHCl_3$ solution and LB films ($CHCl_3$ solution (- - - -); LB films (—); a, 6; b, 14; c, 26; d, 38 layers. Insert: the dependence of absorbance at Soret band on LB films layers).

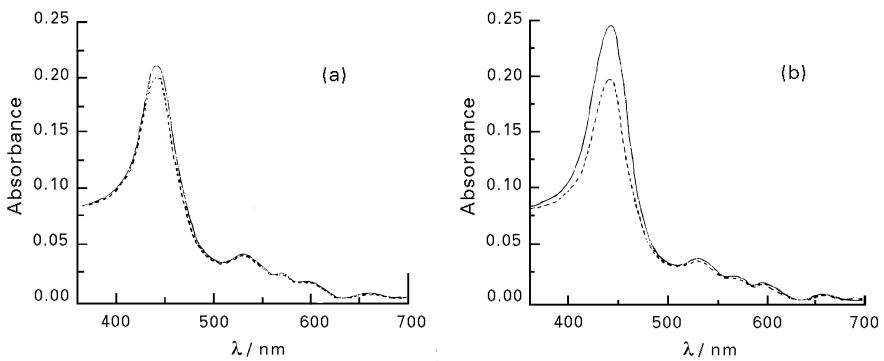

Fig. 5. Polarized UV-vis spectra of $TC_{16}PyP(4)$ LB films (incident light polarized perpendicular (—) and parallel (- - - -) to the dipping direction for (a) $\beta' = 0°$ and (b) for $\beta' = 45°$).

demonstrating that anisotropy exists in the layer plane, and that the $TC_{16}PyP(4)$ macroring is tilted from substrate in a certain angle; quantitative data are listed in Table 1.

According to the Yoneyama equation [8]:

$$\cos^2\theta = \frac{D_0 - \left(1 + D_0 \sin^2\beta\right) D_\beta}{\left(1 - 2\sin^2\beta\right) D_\beta - \left(1 + D_\beta \sin^2\beta\right) D_0} \tag{1}$$

$$\beta = \sin^{-1}(n_1 \sin \beta'/n_2) \tag{2}$$

where $n_1 = 1.0$ (refractive index of air) and $n_2 = 1.429$ (refractive index of porphyrin film) [9].

Using the data in Table 1, the orientation of the porphyrin ring plane was calculated to be at an angel of 27.5°. This value was close to the value of 24° obtained from the π–A isotherm measurement.

3.3 Photoelectric response of $TC_{16}PyP(4)$ LB films

The photocurrent–time response curves are shown in Fig. 6. Curve *a* is the photocurrent–time response curve of SnO_2 OTE itself. Owing to the use of a 390 nm cut-off filter, the blank photocurrent reduced almost to zero. So, the interference of SnO_2 OTE itself could be avoided. Curve *b* is the photocurrent–time response curve of $TC_{16}PyP(4)$ LB films (three layers); the

TABLE 1
Data of Polarized UV-vis Spectra of $TC_{16}PyP(4)$ LB Films[a]

	$A_{\parallel}$	$A_{\perp}$	D	$cos^2\theta$	θ
$\beta' = 0°$	0.208	0.204	1.021	0.785	27.5°
$\beta' = 45°$	0.249	0.199	1.254		

[a] β' is the angle of the incident polarized light, $A_{|}$ and $a_{\perp}$ are the absorbance of $TC_{16}PyP(4)$ LB films for polarized light with electric vectors parallel and perpendicular to the dipping direction, respectively; D is the dichroic ratio (viz $A_{\parallel}/A_{\perp}$).

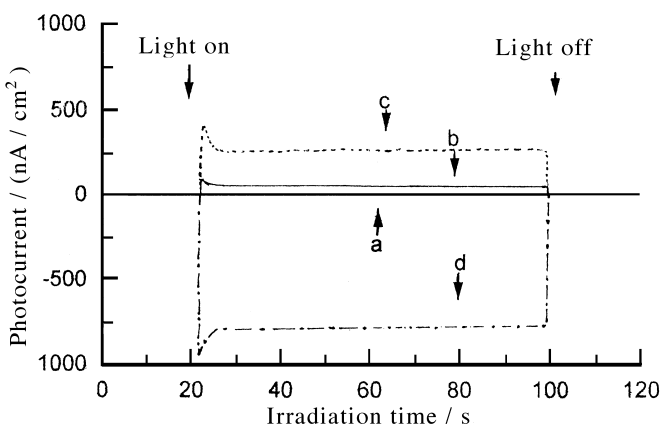

Fig. 6. Photocurrent-time responses of $TC_{16}PyP(4)$ LB films (three layers). (a), Clean SnO_2 OTE, with 0.1 M KCl electrolyte solution; b, c, d, three layers $TC_{16}PyP(4)$ LB films, electrolyte solution: 0.1 M KCl (b), 0.1 M KCl and 80 mM ascodic acid (c), 0.1 M KCl and 1 mM *p*-benzoquinone solution (d).

electrolyte solution was 0.1 M KCl aqueous solution. As seen from the figure, under the short-circuited condition, the photocurrent showed a rapid rise and reached a maximal value of *ca* 60 nA cm^{-2} once the light was turned on, then followed by a exponential decrease and finally reaching a steady value of *ca* 35 nA cm^{-2} 5 s later. On turning off the light, the photocurrent rapidly declined to the zero level. The photocurrent flowed to the SCE electrode, which indicated that electrons were injected from porphyrin molecules to the conduction band of SnO_2. Such behavior had been reported for a Chlorophyll layer deposited on a SnO_2 electrode [10].

The photovoltage-time response curves of $TC_{16}PyP(4)$ LB films were also measured and the results are shown in Fig. 7. Curve *a* is the photovoltage–time response curve of $TC_{16}PYP(4)$ LB films (three layers); the electrolyte solution was 0.1 M KCl aqueous solution contained 80 mM ascorbic acid. The photonvoltage rapidly reach a maximal value of 90 mV once the sample was irradiated. During the illumination, it remained constant. On turning off the light, the photovoltage showed a slow exponential decay. When the electrolyte solution was changed to 0.1 M KCl aqueous solution containing 80 mM *p*-benzoquinone, the photovoltage–time response curve of $TC_{16}PyP(4)$ LB films is as shown in curve *b*. The photovoltage was −110 mV at the moment of irradiation, and remained constant during the illumination. After turning off the light, the photovoltage also showed slow exponential decay, but the direction of the photocurrent is reversed. The large and stable photovoltage response of $TC_{16}PyP(4)$ LB films is an advantageous property, indicating that it is possible for the $TC_{16}PyP(4)$ LB films photovoltaic cell to be used as a potential photovoltaic device.

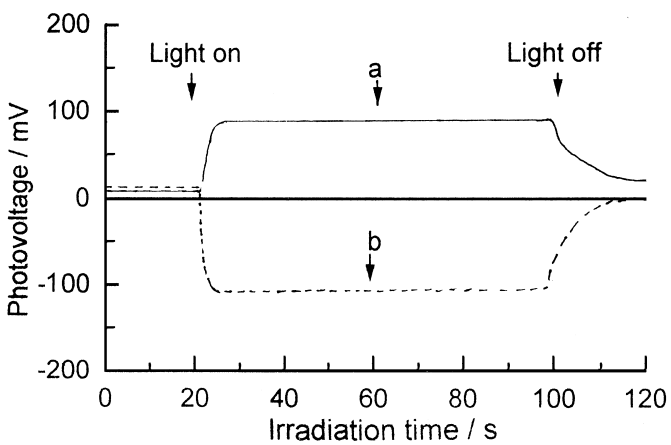

Fig. 7. Photovoltage-time responses of $TC_{16}PyP(4)$ LB films (three layers). Electrolyte composition: (a) 0.1 M KCl and 80 mM ascodic acid solution; (b) 0.1 M KCl and 1 mM *p*-benzoquinone aqueous solution.

We considered that the photoelectric response of $TC_{16}PyP(4)$ LB films was due to a photo-induced charge transfer mechanism. If this is true, the presence of electron donors or acceptors in the electrolyte solution would certainly affect the efficiency and speed of the photo-induced charge transfer. Therefore, the photocurrent differences of $TC_{16}PyP(4)$ LB films were compared in either the presence or absence of electron donors or acceptors in the electrolyte solution; the results are shown in Fig. 6. When an electron donor, ascorbic acid (80 mM), was added to the 0.1 M KCl electrolyte solution, the maximal photocurrent and steady photocurrent increased to 400 nA cm^{-2} and 250 nA cm^{-2}, respectively. Generally, the photocurrent increases are due to supersensitization, which has been previously reported in Chlorophyll **a** and **b** LB film electrochemical cells [10]. Two possible schemes are possible for the supersensitization: (i) the electron is injected to the conduction band of the SnO_2 electrode from the excited $TC_{16}PyP(4)^*$, producing the cation radical $TC_{16}PyP(4)^{+\bullet}$, which is reduced by abstracting an electron from the electron donor, resulting in the regeneration of the photoactive state and (ii) owing to the presence of the electron donor, the excited $TC_{16}PyP(4)^*$ abstracts an electron from the electron donor, giving the anionic radical $TC_{16}PyP(4)^{-\bullet}$ which has a stronger ability to donate electrons than $TC_{16}PyP(4)^*$; the efficiency of electron injection to the conduction of SnO_2 electrode is thus increased.

Similarly, with the addition of the electron acceptor *p*-benzoquinone (1 mM), the maximal photocurrent and steady photocurrent were increased to -950 nA cm^{-2} and -800 nA cm^{-2}, respectively, but, it is noticeable that the direction of the photocurrent is reversed. The reason is that *p*-benzoquinone captures directly the electron of the excited $TC_{16}PyP(4)^*$, producing the cation radical $TC_{16}PyP(4)^{+\bullet}$, leading to electron injection from the conduction band of SnO_2 to the reduced porphyrin $TC_{16}PyP(4)^{-\bullet}$. Similar phenomena have been observed in the R-phycoerythrin/semiconductor electrochemical cell [11].

A schematic diagram for the electron-transfer processes at a $TC_{16}PyP(4)$ monolayer deposited on SnO_2 electrode is illustrated in Fig. 8 The values of pH and the electrode potential are tentatively assumed to be 7.0 and -0.1 V vs SCE, respectively. At this pH, the flatband potential of SnO_2 is situated at -0.45 V vs SCE, and hence the potential drop 70 within the space charge layer amounts to 0.55 V. Using the $TC_{16}PyP(4)$ oxidation potential of $+0.88$ V vs SCE and the singlet excitation energy of $+1.93$ V, one obtains the oxidation potential of $TC_{16}PyP(4)^*$ as -1.05 V vs SCE. Since this level is energetically higher than the conduction band of SnO_2, the electron-transfer paths in Fig. 8 are possible, The direction of electron-transfer is shown in Fig. 8 by solid lines, and the electron is injected from the excited $TC_{16}PyP(4)^*$ or oxidized $TC_{16}PyP(4)^{+\bullet}$ to the conduction band of SnO_2 in the presence or absence of electron donor (D/D^+) in the electrolyte solution.

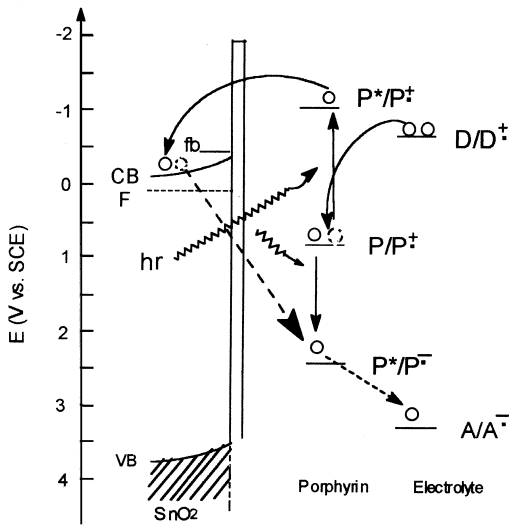

Fig. 8. Schematic diagram for the electron transfer at $TC_{16}PyP(4)$ monolayer on SnO_2 E_{CB}, E_B, E_f, and E_{fb} denote the potentials (V vs SCE) of the conduction band, valence band, Fermi level, and flatband of SnO_2, respectively.

The dash lines indicate the electron-transfer direction in the presence of an electron acceptor (A/A^-). In this case, electron injection from the conduction band of SnO_2 to the reduced $TC_{16}PyP(4)^{-\bullet}$ leads to the reverse photocurrent, in comparison with the former condition.

4 CONCLUSIONS

The electrochemical cell of $TC_{16}PyP(4)$ monolayer deposited on SnO_2 OTE by LB film technique has an evident photovoltaic effect. The photocurrent increases in the presence of electron donor or acceptor in the electrolyte solution, indicating that the photovoltaic effect of $TC_{16}PyP(4)$ perhaps originates from the photo-induced charge transfer between $TC_{16}PyP(4)$ molecules and SnO_2 semi-conductor. From the π–A isotherm and polarized absorption spectrum, it is inferred that the porphyrin ring is oriented at an angle of about 25° against the aqueous surface, as well as the substrate plane.

ACKNOWLEDGEMENTS

Project (59573010) supported by the National Natural Science Foundation of China. This work was supported by the Laboratory of Organic Solids of the Chinese Academy of Sciences.

REFERENCES

1. Merrit, V. Y, and Hovel, H. J., *Appl, Phys. Lett.*, 1976, **29**, 414–415.
2. Kampas, F. J., Yamashita, K. and Fajer, J., *Nature*, 1980, **284**, 40–42.
3. Harriman, A., Porter, G. and Richous, M. C., *J. Chem. Soc. Faraday Trans. II*, 1981, **77**, 833–844.
4. Snow, A. W. and Jaarvis, N. L., *J. Am. Chem. Soc.*, 1984, **106**(17), 4706–4711.
5. Desormeaux, A., Max, J. J. and Leblance, R. M., *J. Phys. Chem.*, 1993, **97**, 6670–6678.
6. Okuno, Y., Ford, W. E. and Calvin, M., *Synthesis*, 1980, **7**, 537–539.
7. Scheidt, W. R., *Acc. Chem. Res.*, 1977, **10**, 339–345.
8. Yoneyama, M., Sugi, M., Saito, M., *Jpn. J. Appl. Phys.*, 1986, **25**, 961–965.
9. Vandevyver, M., Barraud, A., Raudel-Teixier, M. P. and Gianotti, C., *J. Colloid and Interface Scence*, 1982, **85**(2), 571–585.
10. Miyasaka, T., Watanabe, T., Fujishima, A. and Honda, K., *J. Am. Chem. Soc.*, 1978, **100**(21), 6657–6665.
11. He, J. A., Jiang, L. J., Bi, Z. C. and Jiang, L., *Scientia in China. Ser. B*, 1996, **39**(4), 387–397.